Journal of Alloys and Compounds 854 (2021) 157152

Contents lists available at ScienceDirect

Journal of Alloys and Compounds

journal homepage: http://www.elsevier.com/locate/jalcom

Cauliflower-shaped Bi_2O_3—ZnO heterojunction with superior sensing performance towards ethanol

Peng Wang [a], Su-Zhen Wang [a], Ya-Ru Kang [a], Zhong-Sen Sun [a], Xue-Dong Wang [c], Yu Meng [a], Ming-Hui Hong [d], Wan-Feng Xie [a, b, d, *]

[a] School of Electronics & Information, Qingdao University, Qingdao, 266071, China
[b] State Key Laboratory of Bio-Fibers and Eco-Textiles, Qingdao University, Qingdao, 266071, China
[c] Jiangsu Key Laboratory for Carbon-Based Functional Materials & Devices, Institute of Functional Nano & Soft Materials (FUNSOM), Soochow University, Suzhou, Jiangsu, 215123, China
[d] Department of Electrical and Computer Engineering, National University of Singapore 4 Engineering Drive 3, 117576, Singapore

ARTICLE INFO

Article history:
Received 1 June 2020
Received in revised form
8 September 2020
Accepted 10 September 2020
Available online 12 September 2020

Keywords:
Semiconducting metal oxide
ZnO
p-n junction
Ethanol
Resistive sensor

ABSTRACT

Gas sensors based on metal oxide semiconductors have attracted great interest in the sensing of organic volatile compounds gas due to their easy fabrication, effective cost, and good stability. Herein, we rationally design ethanol gas sensors based on *p*-Bi2O3 and *n*-ZnO heterostructure with clear interfaces, which exhibit excellent response of 21.6 towards 100 ppm ethanol, wide concentration detection range from 1 to 500 ppm, working temperature as low as 175 °C, short response time of 7 s, and recovery time of 8 s at 100 ppm of ethanol. Moreover, the selectivity of Bi2O3/ZnO sensor towards ethanol is much better than that of other organic volatile gases. The relationship between the origin of superior sensing performances towards ethanol and the sharp interfaces of *p*-Bi2O3/*n*-ZnO heterostructure are also systematically investigated. On the other hand, it is also demnostrated that the tetragonal phase β-Bi_2O_3 has positive effect on the sensing performance of Bi_2O_3/ZnO composite.

1. Introduction

Owing to the rapid growth of the Web of things (WOT) and Internet of vehicles (IOV), modern technologies based on sensors are being extensively developed and applied to promote industrial evolution, optimize environmental quality and living standard of humans, etc [1–3]. As far as the sensors are concerned, chemiresistive type sensors based on metal oxides semiconducting (MOSCs), such as ZnO [4], Bi_2O_3 [5], MoO_3 [6], α-Fe_2O_3 [7], WO_3 [8], SnO_2 [9], In_2O_3 and their nanocomposites, possess good properties, including sensing response, stability, low product cost, and simple accomplishment for precise controlled in real time, which make them competitive to be utilized extensively in modern industry, medical treatment and people's livehood aspects [4,10,11].

Volatile organic compounds (VOCs), such as alcohol, methanol, ethylene glycol and other aromatic carbohydrates, are unhealthy to human body due to their nature to damage mucous membranes and respiratory tracts [12,13]. But, people's olfactory system is not sensitive enough to accurately detect a few VOCs. Therefore, it is highly desirable to develop a superior gas sensor not only for the detection of flammable, toxic and explosive VOCs that may come from emission and leakage, but also for the quality control of living environment, food inspection and medical diagnostics [14]. Ethanol (C_2H_5OH), for example, is an important raw material in brewing industry. In recent years, researches on gas sensors toward ethanol have attracted extensive attentions due to their various applications in drunken-driving, food packaging monitoring, and leakage-detecting from chemical factories [15,16]. Furthermore, a lot of C_2H_5OH leakage would trigger explosion in distilleries and bonded storehouses [5]. Therefore, low operating temperature, fast, selective, and highly sensitive ethanol sensors are still highly desired.

Due to the simplicity in operation, low production cost, flexibility in production and small size, the sensors based on metal oxide semiconductors (MOSCs) have received strong attention [2,6,8]. The operating mechanism is that in which the target gas molecules are adsorbed and react with the surface chemisorbed oxygen species of the gas sensing material, which induces an

* Corresponding author. School of Electronics & Information, Qingdao University, Qingdao, 266071, China.
E-mail address: wfxie@qdu.edu.cn (W.-F. Xie).

https://doi.org/10.1016/j.jallcom.2020.157152
0925-8388/

evident change of sensor resistance [12]. To further improve the gas sensing functionality, such as operating temperature, sensitivity, selectivity, stablity, and reprodcibility. Some techniques have been proposed recently to solve these disadvantages [3,8,14]. Firstly, for example, to synthesize and utilize novel nanostructured materials with high specific surface-to-volume ratios [16,17]; Secondly, surface modification by doping or decorating approaches with noble metals, such as Pt, Pd, Au, Ag and Cr, transition element and metal oxide particles (Bi_2O_3, TiO_2, Y) [1,18–22]; Thirdly, to form heterostructure, including *p*-*n*, *n*-*n*, and *p*-*p* junctions via grafting stragety, for example, core-shell structure and surface decoration by metal oxide nanoparticles, here, *p* refer to *p*-type semiconductor, *n* stand for *n*-type semiconductor [10,23] As listed in Table 1, a numerous of MOSCs have been used for the latter purpose, but there have been few reports on Bi_2O_3/ZnO heterojunction sensors toward ethanol at low working temperature. On the other hand, the systematic discussion on the sensing mechanism based on the *p*-Bi_2O_3/n-ZnO heterostructures is scarce.

According to the best of our knowledge, the research on Bi-doped ZnO [30], Bi_2O_3-core/ZnO-shell structures [31], and ZnO/Bi_2O_3 nanocomposites are still the hot research interests [32]. For example, Lee's group fabricated 1D Bi_2O_3-core/ZnO-shell nanostructures by thermal evaporation and atomic layer deposition (ALD), which exhibited novel photoluminescence (PL) properties [33]; Later, Lee's group studied the light-activated gas sensing of Bi_2O_3-core/ZnO-shell nanobelt toward NO_2 [34]; Subramanian et al. reported that a new heterostructured Bi_2O_3/ZnO, which exhibited higher photocatalytic performace for the degradation of Acid Black 1 under the irradiation of UV light [35]; In 2015, Yi et al. prepared *p*-Bi_2O_3/*n*-ZnO heterojunctions, and photogenerated charge transfer properties and enhanced visible-light photocatalytic activity were investigated [36]; Additionally, Xu et al. proposed a novel method to achieve epitaxial growth of δ-Bi_2O_3 layers onto the 11–20 nanoscale facets of ZnO nanowires [37]; Recently, Zahirullah and his group prepared Bi doped ZnO thin films, which shows a certain response toward ethanol at 400 °C [30].

In this work, we display a facile strategy to synthesize *p*-Bi_2O_3/*n*-ZnO heterojunction with novel cauliflower shape via hydrothermal and calcination methods. It is worth mentioning that incorporation of 3 mol% Bi_2O_3 into Bi_2O_3/ZnO nanocomposites can proportionally enhance the sensing performance toward C_2H_6O. This work shows that high efficient Bi_2O_3/ZnO sensing materials could be synthesized via facile hydrothermal, and it also offers a new insight into the rational design and fabrication of sensing materials with heterojunction structures for advanced electronic devices.

2. Experimental

All analytical grade reagents and chemicals were commercially purchased from Aladdin (Shanghai, China), and used as received without any further purification.

In this study, the Bi_2O_3/ZnO nanocomposites were prepared by a two-step synthetic route. Typically, 0.75 mmol $Zn(NO_3)_2 \cdot 6H_2O$, 0.5 mmol hexadecyltrimethylammonium bromide ($C_{19}H_{42}BrN$) was added into 50 mL mixture solvant of deionized water and absolute ethyl alcohol (the ratio of volume:1:1) with stirring; Secondly, 0.0225 mmol $Bi(NO_3)_3 \cdot 5H_2O$ and 3 mmol ammonium fluoride (NH_4F) were added into the above solution slowly under the vigorously stiring for 4 h; Thirdly, 50 μl HCl was added into the solution with constant stirring; Finally, the homogeneous solution was transferred into a 60 mL Teflon-lined autoclave. Then, the autoclave was maintained at 120 °C for 24 h. Then, the precipitates were collected by centrifugation and were rinsed repeatedly with deionized water and absolute ethanol several times. The products were dried at 80 °C for 10 h and sintered at 500 °C for 2 h. In this study, the as-prepared samples in the subsequent discussion are expressed as Bi_2O_3(x%)/ZnO, where x% refers to the molar ratio of Bi in Bi_2O_3/ZnO composites, the molar ratios of Bi are 0%, 1%, 3%, 5%, and 100%, respectively.

The preparation of home-made gas devices: Firstly, the pure ZnO and the Bi_2O_3/ZnO nanocomposites were mixed with absolute ethanol to form paste; Secondly, the paste was dropcoated orderly onto the surface of a ceramic tube with four platinum electrodes for several times to obtain uniform coating. The ceramic tube coated with pure ZnO and Bi_2O_3/ZnO nanocomposites were welded to a special six-polar pedestal. In addition, the sensors were aged at 400 °C for 7 days to improve the thermal stability of the gas sensor resistance. The gas sensing performances were measured by a system (WS-30A) [38]. In addition, the sensing response was calculated by the resistance ratio of the sensor resistance in aim gases (R_g) to that in fresh air (R_a). The response/recovery time was defined as the time taken to reach 90% variation in the sensor resistance.

Powder X-ray diffraction (XRD) patterns were collected with a Bruker AXS (D8, advance) diffractometer using Cu Kα1 (λ = 0.1540598 nm) radiation at a scanning rate of 1° min^{-1}. The morphologies of the samples are investigated by a field emission scanning electron microscope (FESEM, Zeiss Gemini 500) and a high resolution transmission electron microscope (HRTEM) JEOL-2100F. The XPS measurements were recorded with a Termo Scientific Escalab 250xi instrument equipped with a monochromatic Al Kα source.

3. Results and discussion

The morphology of the Bi_2O_3/ZnO nanocomposite after sintering was determined by FESEM observations. Fig. 1a shows a general synthesis process of the sensing materials. Herein, we firstly obtained Bi_2O_3/ZnO precursors via hydrothermal processes, and then the precursors were calcined in air directly. Finally, the Bi_2O_3/ZnO nanocomposites could be obtained. As shown in the low resolution FESEM images of Fig. 1b and c, it can be evidently seen that a large number of sub-micrometer scale Bi_2O_3/ZnO nanospheres were successfully synthesized. Interestingly, the 3D (three dimensional) Bi_2O_3/ZnO sub-microspheres consisted of many tightly aggregated 3D nanoparticles, which are very closly to the surface of the blooming cauliflower, as shown in the high magnitude FESEM of Fig. 1d. Furthermore, some mesopores and obvious boundaries/

Table 1
Sensors based on metal oxide semiconductors heterojunction toward ethanol.

Materials	Concn (ppm)	Operating temp (°C)	Response (R_a/R_g)	τ_{res}/τ_{recov} (s)	References
$Zn_3(VO_4)_2$	100	400	11.45	–	[24]
ZnO/Ag	20	370	101.8	15/20	[25]
In_2O_3/Bi_2O_3	200	200	17.5	24/180	[5]
ZnO/In	100	250	88	25/10	[26]
Bi_2WO_6	100	300	34.6	-/27	[27]
ZnO/NiO	500	400	37.5	2.1/4.1	[28]
$CuBi_2O_4$	1000	400	10.4	–/–	[29]

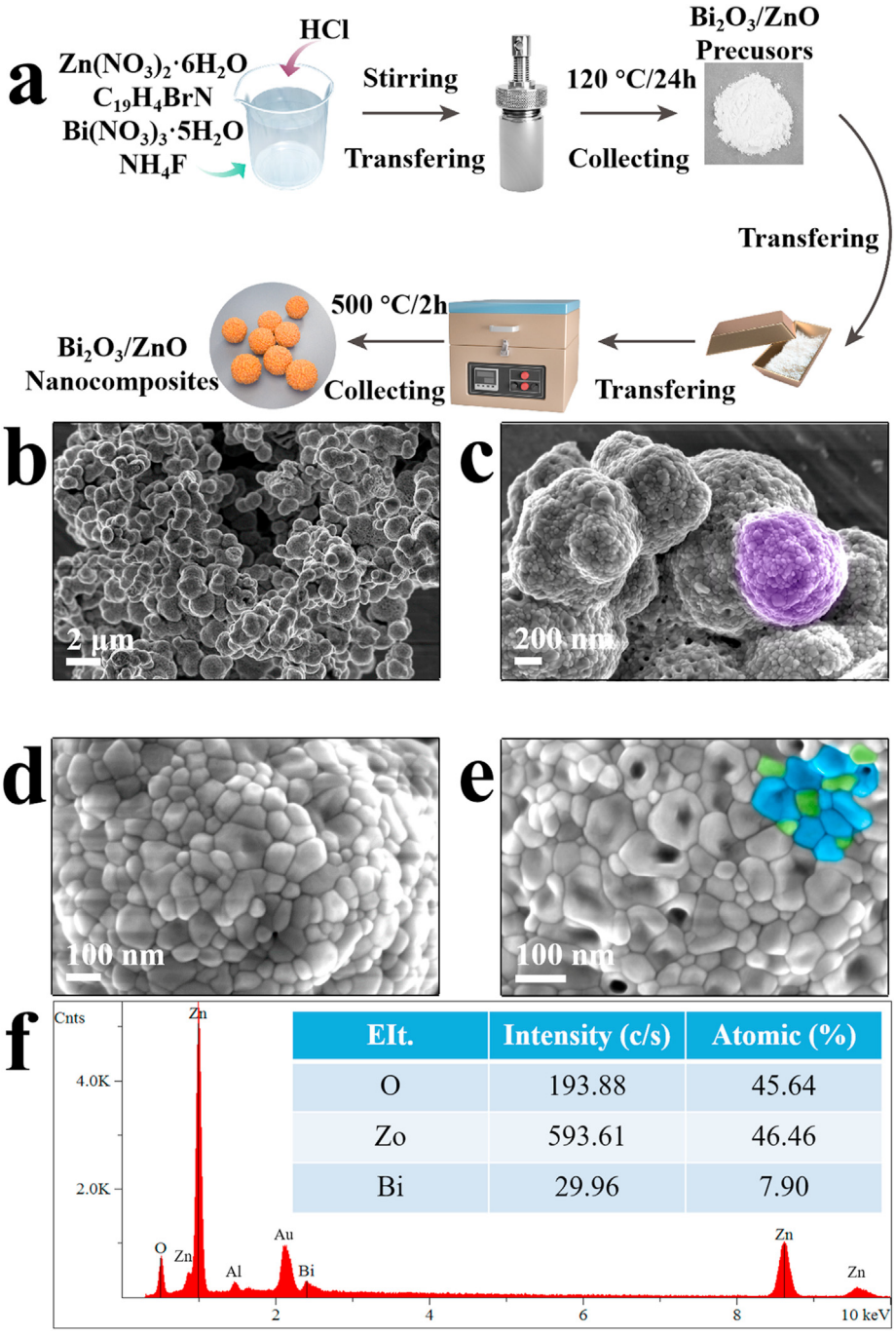

Fig. 1. (a) Sketch of the general synthesis processes of cauliflower-shaped Bi_2O_3/ZnO nanocomposites; (b) and (c) The low magnification FESEM images of Bi_2O_3/ZnO products; (d) and (e) The high resolution FESEM images of Bi_2O_3/ZnO nanocomposites. (f) The EDS pattern and relative content of Zn, Bi and O.

interfaces can be observed clearly, as shown in Fig. 1e. Compositions and molar ratio of Bi_2O_3(3%)/ZnO nanocomposite have been determined using EDS as shown in Fig. 1f and the inset Table. The EDS spectrum shows that components of the Bi_2O_3(3%)/ZnO are, Zn, Bi and O. It worthy to note that the Bi content approaches the expected propotion of 3%.

To further investigate the microstructure information of the Bi_2O_3/ZnO composite, a HRTEM was employed to measure the heterojunction properties of the sample. As evidently shown in Fig. 2a, it can be observed that there is a very sharp and clear heterointerface between ZnO and Bi_2O_3, which is well consistent with the result of the FESEM measurements. On the other hand, according to the elemental mapping images, the Zn and Bi elements uniformly distribute on one side of each other. In this image, the Bi element is on the left side (Fig. 2b), and the Zn element is on the right side (Fig. 2c). In addition, the elemental mapping image (Fig. 2d) indicates the uniform distribution of O onto the surface of Bi_2O_3/ZnO nanocomposites. Fig. 2e dispalys a overall image including all the elements of Bi, Zn and O of Bi_2O_3/ZnO nanocomposite, it can be seen that the interface between Bi_2O_3 and ZnO is particularly clear and sharp, which is beneficial to sensing properties. Besides, the EDS mapping images with very low-resolution were investigated to further manifest the distribution of the elements in Bi_2O_3(3%)/ZnO nanocomposite, see Fig. S1 (Supporting Information), which shows

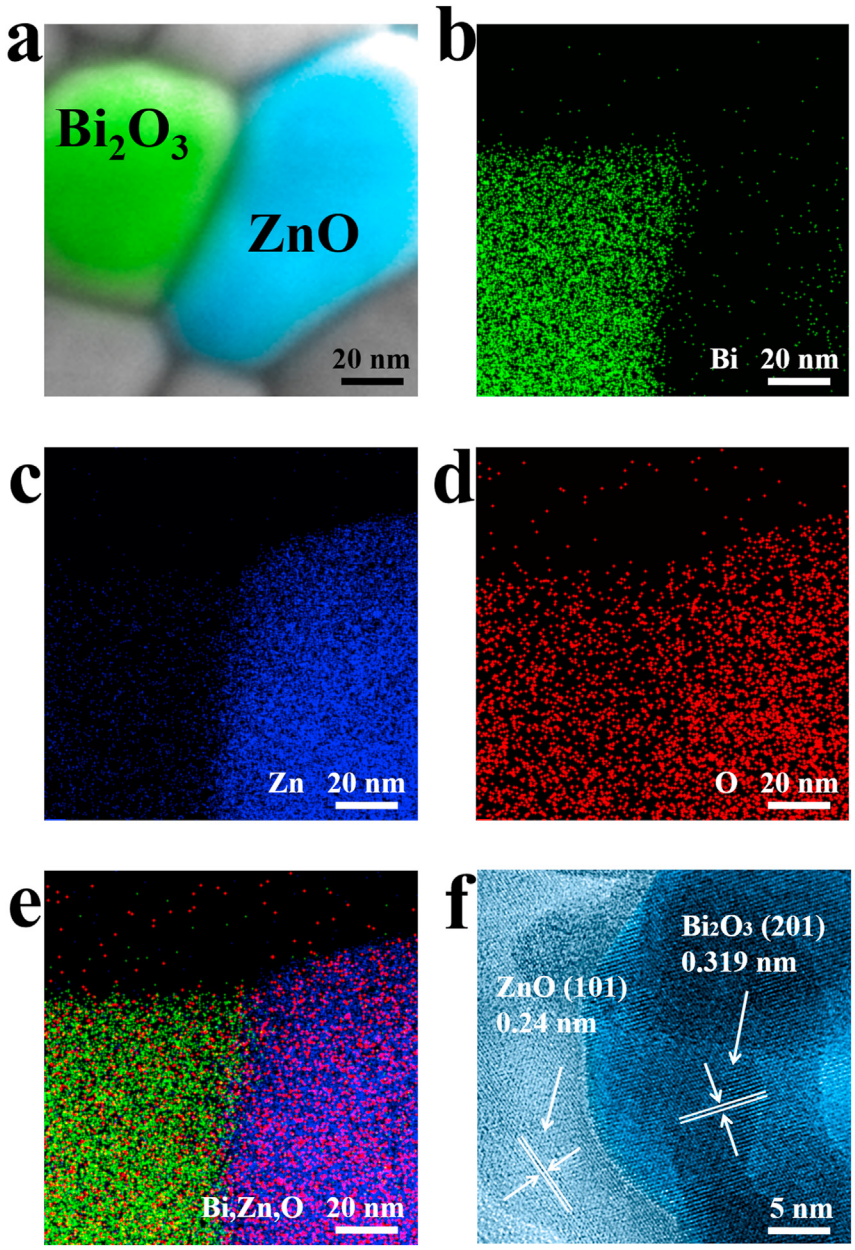

Fig. 2. (a) The HRTEM image of Bi_2O_3/ZnO heterojunction; (b–e) EDXS mapping of (b) Bi, (c) Zn, (d) O, and (e) The overall mapping image including all the elements of Bi, Zn and O; (f) Lattice fringes image of Bi_2O_3/ZnO nanocomposite.

the Zn, Bi and O contents, and the Bi intensity is much weaker than that of Zn, similar result was demonstrated in Fig. 1f. Additional microstructural analysis was performed on the Bi_2O_3/ZnO nanocomposite using HRTEM. As Fig. 2f depicts, a representative image of the Bi_2O_3 shows a typical lattice fringe spacing of 0.319 nm, which is the (201) plane of the Bi_2O_3 [39]. Moreover, the lattice fringe spacing of ZnO is 0.24 nm, which correspondes to the (101) plane [40].

In the X-ray diffraction (XRD) patterns, the pristine ZnO, Bi_2O_3 and Bi_2O_3/ZnO nanocomposites show well resolved diffraction peaks in the range of 10° - 80° (Fig. 3). The 2θ values of as prepared ZnO (the black curve) at 31.77°, 34.42°, 36.25°, and 76.95° correspond to (100), (002), (101), and (202) diffraction planes of hexagonal phase wurtzite ZnO (PDF#89–0511) [40–42]. The pristine Bi_2O_3 (the orange) exhibits monoclinic phase of α-Bi_2O_3 (PDF#71–2274) as can be observed from the spectra of Fig. 3. And the characteristic 2θ values at 27.47° (120), 33.03° (121) can be

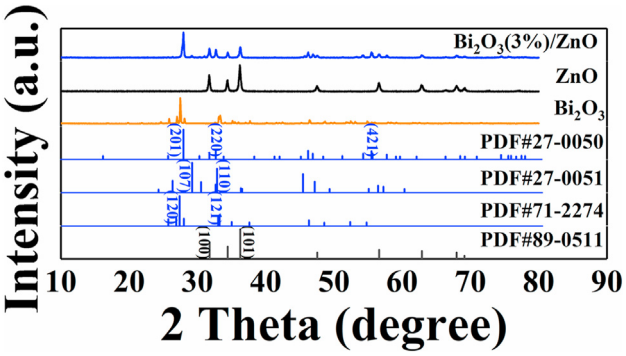

Fig. 3. XRD patterns of Bi_2O_3 (3%)/ZnO nanocomposite (the blue curve), pure ZnO (the black) and the pure Bi_2O_3 (the orange curve), respectively.

assigned to monoclinic α-Bi_2O_3 (PDF# No. 71–2274) [43]. For Bi_2O_3(3%)/ZnO nanocomposite, as shown in Fig. 3 (the blue pattern), it contains hexagonal phase wurtzite ZnO (PDF#89–0511), monoclinic phase of α-Bi_2O_3, and tetragonal phase Bi_2O_3, but there two kinds of Bi_2O_3, that is β-Bi_2O_3 (PDF#27–0050) and non-stoichiometric phase of $Bi_2O_{2.33}$ (PDF#27–0051). These results are similar to those reported in some other literature [5,39,44,45]. As we all known, the formation of $Bi_2O_{2.33}$ would introduce rich defects including lattice distortion and oxygen vacancies, which are benefit to the sensing performance [5,45]. Additionally, to further investigate the microstructure of Bi_2O_3/ZnO nanocomposites, the XRD patterns of Bi_2O_3(15%)/ZnO, Bi_2O_3(30%)/ZnO, Bi_2O_3(50%)/ZnO, and Bi_2O_3(75%)/ZnO composites were measured, respectively, see Fig. S2 (supporting information). From the results, the proportion of monoclinic α-phase is obviously increasing with the increase of content of Bi_2O_3 in the Bi_2O_3/ZnO composites. For Bi_2O_3(75%)/ZnO, the main phase is the monoclinic α-Bi_2O_3. Furthermore, the diffraction peaks of the pristine ZnO and Bi_2O_3/ZnO nanocomposite were sharp and intense, indicating the highly crystalline character of the samples. On the other hand, on evident solid-state solutions are formed between two oxides of Bi_2O_3 and ZnO.

Moreover, the chemical composition of the Bi_2O_3(3%)/ZnO nanocomposite was studied by X-ray photoelectron spectroscopy (XPS) analysis, and the corresponding results are shown in Fig. 4. The Bi 4f spectrum in Fig. 4a displays two symmetric peaks located at 160.9 eV and 164.7 eV, which are the characteristic peaks of surface Bi^{3+} species [46]. Additionally, as displayed in Fig. 4b, the Zn $2p_{3/2}$ locates at 1022.2 eV and the Zn $2p_{1/2}$ is at 1045.3 eV, with an interval of approximately 23.1 eV, indicating a normal form of Zn^{2+} in the Bi_2O_3/ZnO nanocomposite [37,47]. Fig. 4c reveals that the O 1 s peak can be fitted by two different peaks. The peaks at 530.1 eV and 531.8 eV could be attributed to crystal lattice oxygen (O^{2-}) ions and adsorbed oxygen species (O_2^-, O^-, and O^{2-}) [47,48].

Fig. 5a shows the inner working circuit of the home-made sensor. It is generally known that the performance of MOSCs based gas sensor is greatly influenced by its operating temperature [5,7,18]. In order to investigate the optimum working temperature, the sensing responses of pure ZnO and Bi_2O_3/ZnO nanocomposites gas sensors toward 100 ppm C_2H_6O were tested as a function of operating temperature from 100 to 300 °C, as shown in Fig. 5b. It is clear that the responses of the Bi_2O_3(3%)/ZnO and Bi_2O_3(5%)/ZnO increase faster than that of pristine ZnO and Bi_2O_3(1%)/ZnO with the increase of ethanol concentration. The Bi_2O_3(3%)/ZnO and Bi_2O_3(5%)/ZnO based sensors reach the maximum response at 175 °C, the pure ZnO and Bi_2O_3(1%)/ZnO sensors approach the maximum response at 250 °C. Subsquently, the responses of all the sensors begin to descent evidently with the gradually increase of the temperature, especially for Bi_2O_3(3%)/ZnO. The maxmium responses of the Bi_2O_3(3%)/ZnO and pure ZnO based sensors are 21.2 at 175 °C and 8.7 at 250 °C, respectively. According to the literature, different gases have different energies to adsorption/desorption on the surface of sensing material [10,13]. At lower temperature, the response of Bi_2O_3/ZnO sensor may be restricted by the speed of chemical reaction. Similarly, the response is restricted by the speed of diffusion of the gas molecules at high temperature such as from 250 °C to 300 °C. At optimum temperature, however, the speeds of the two processes close to approximate dynamic equilibrium, which benefits to the sensor response reacheing its maximum. Furthermore, the reaction rate between ethanol and adsorbed oxygen species will be accelerated by the synergistic effect of Bi_2O_3/ZnO heterostructure, which leads to the high response to ethanol. Specifically, the optimum molar ratio of Bi/Zn has the best synergistic function due to the formantion of tetragonal phase of β-Bi_2O_3 and $Bi_2O_{2.33}$ in the Bi_2O_3(3%)/ZnO composite. In addition, the maximum response to pure ZnO, Bi_2O_3(1%)/ZnO and Bi_2O_3(5%)/ZnO are 8.7, 13.5 and 11.5 at their corresponding optimum temperature, respectively. Thus, the optimum operating temperature of 175 °C and doping ratio (Bi/Zn molar ratio is 3:97) were chosen to further examine the other characteristics of the Bi_2O_3/ZnO based sensor. In addition, it can be observed that there is no evident response towards 500 ppm ethanol at 175 °C of Bi_2O_3 based sensor, see Fig. S3 (Supporting Information). According to the best of knowledge, the pure Bi_2O_3 sensor towards ethanol has not been reported till now.

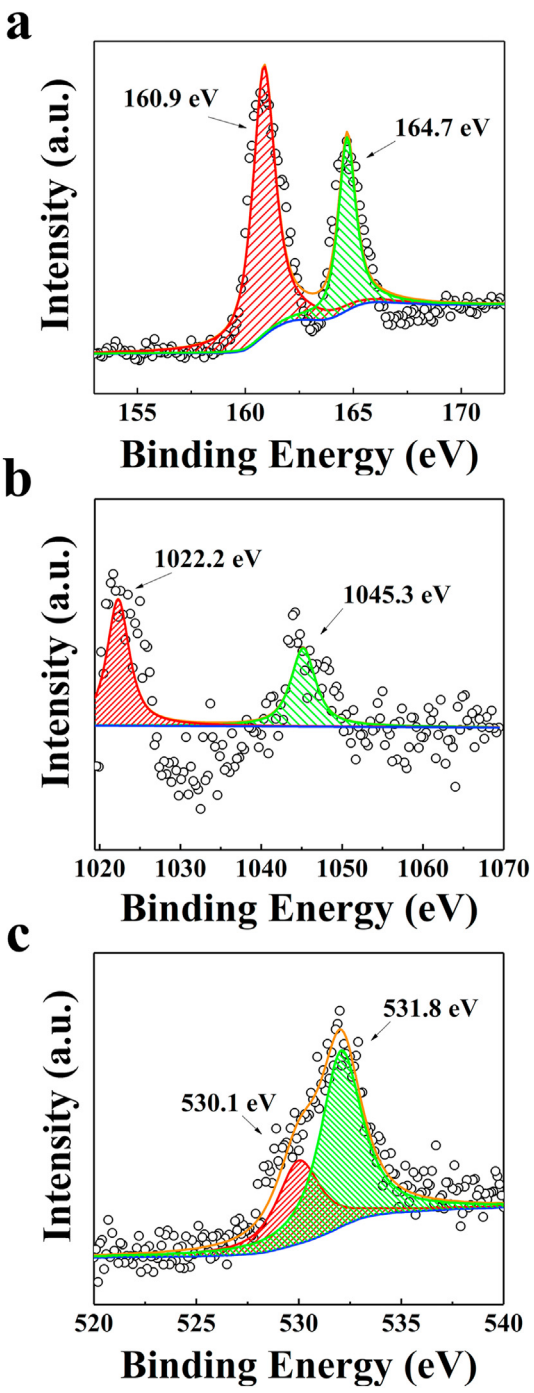

Fig. 4. XPS spectra of Bi_2O_3/ZnO nanocomposite: (a) Bi 4f, (b) Zn 2p, and (c) O 1s XPS spectrum, respectively.

Fig. 5c gives the dynamic response and recovery characteristics of the sensors based on pristine ZnO and Bi_2O_3(3%)/ZnO

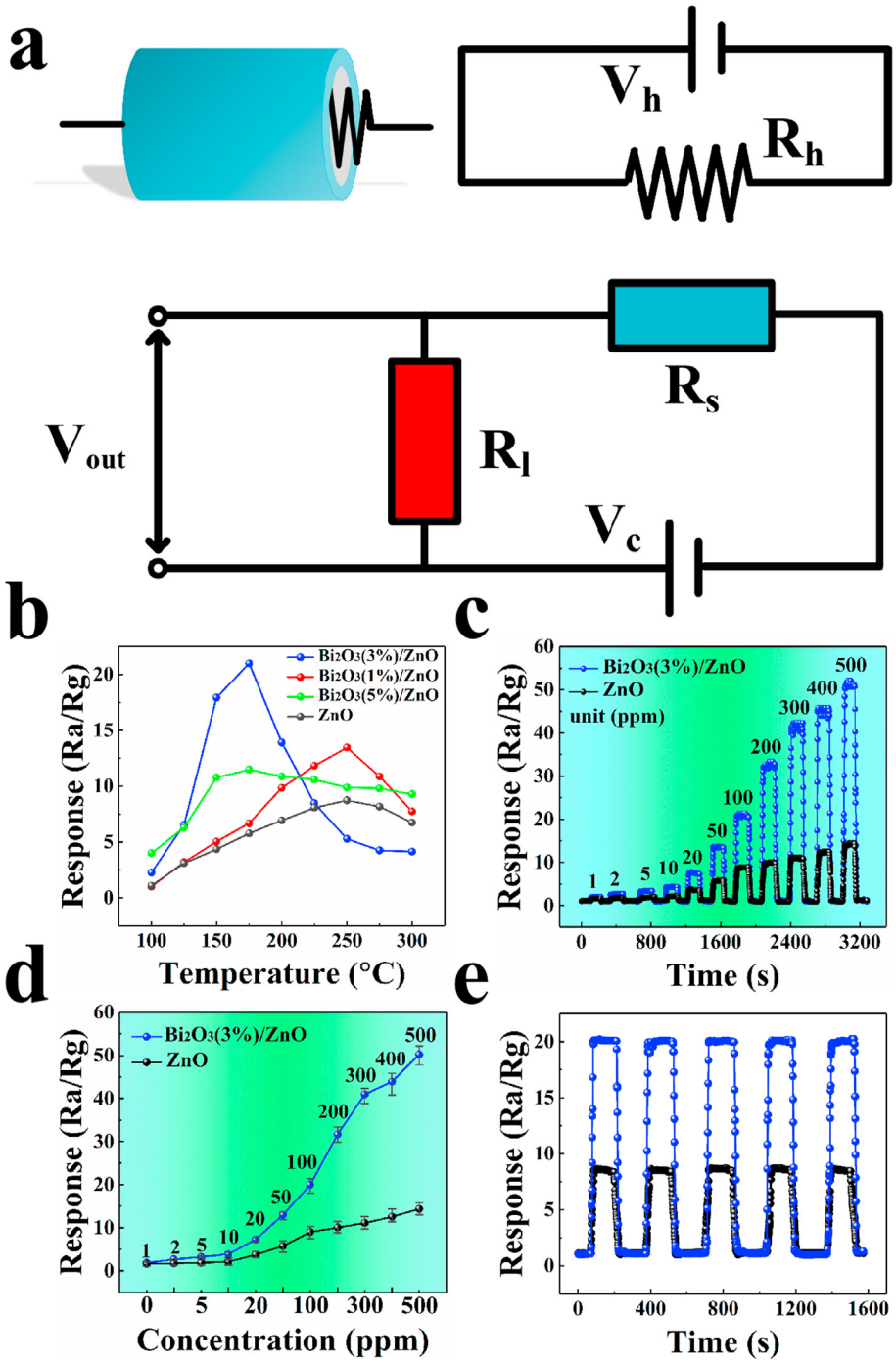

Fig. 5. (a) The gas sensor structure, wire connection, the schematic of the testing circuit; (b) Sensing performances of the gas sensors toward 100 ppm ethanol gas at different operating temperatures; (c) Dynamic resistance changes of the pristine ZnO and Bi_2O_3(3%)/ZnO nanocomposite sensors when exposed to various ethanoles gas toward 1–500 ppm ethanol at 250 °C and 175 °C, respectively; (d) The response vs gas concentrations for Bi_2O_3(3%)/ZnO and ZnO sensors, respectively; (e) Repeatability test of the pristine ZnO and Bi_2O_3(3%)/ZnO nanocomposite sensors to 100 ppm of ethanol at 250 °C and 175 °C, respectively.

nanocomposite to different alcohol concentrations from 1 to 500 ppm at 250 °C and 175 °C, respectively. Obviously, the Bi_2O_3(3%)/ZnO exhibits the superior response and recovery natures to ethanol, as shown in Fig. 5c. Thus, it can be demonstrated that the cauliflower-shaped nanostructure can produce more cusps on the surface of Bi_2O_3(3%)/ZnO nanocomposite, which can play as active sites for ethanol. Additionally, the response of the gas sensor is decided by the surface reaction rate with the increasing concentration of ethanol. In low concentration from 1 to 20 ppm, the climb of sensor response is slow. But at 50 ppm, the response of Bi_2O_3(3%)/ZnO is rising sharply. When the alcohol concentration reaches to 500 ppm, and the response still keeps increasing, see Fig. 5d. The detailed responses of Bi_2O_3(3%)/ZnO and pristine ZnO are listed in Table 2 and Table 3, respectively. We can conclude that the Bi_2O_3(3%)/ZnO shows approximately 3 times higher response than pristine ZnO from the tables. Therefore, the Bi_2O_3(3%)/ZnO sensor has potentiol application prospect. For comparison, the dynamic response and recovery curves of Bi_2O_3(1%)/ZnO and Bi_2O_3(5%)/ZnO

Table 2
The responses of Bi_2O_3(3%)/ZnO sensor at 175 °C.

Concentration (ppm)	1	2	5	10	20	50
Response	2.0	2.7	3.4	4.3	7.5	13.5
Concentration (ppm)	100	200	300	400	500	
Response	21.1	32.2	41.8	45.1	50.0	

Table 3
The responses of pristine ZnO sensor at 250 °C.

Concentration (ppm)	1	2	5	10	20	50
Response	1.3	1.5	1.8	2.1	3.6	4.7
Concentration (ppm)	100	200	300	400	500	
Response	8.8	9.2	11.0	12.5	14.1	

are given, see Figs. S4 and S5 (Supporting Information), respectively. It can be concluded that Bi_2O_3(3%)/ZnO has superior sensing performances. Fig. 5e shows a typical repeatability performance of the Bi_2O_3/ZnO and pristine ZnO sensors to 100 ppm ethanol at 175 °C and 250 °C, respectively. Obviously, the response (S_r = 21.0) of Bi_2O_3(3%)/ZnO sensor is much higher than that (S_r = 8.5) of ZnO sensors, because of the cauliflower shaped nanostructures of Bi_2O_3/ZnO and sharp interface between ZnO and Bi_2O_3. Similarly, the repeatability of Bi_2O_3(1%)/ZnO and Bi_2O_3(5%)/ZnO sensors were measured toward 100 ppm ethanol at their corresponding working temperatures, respectively. Evidently, both Bi_2O_3(1%)/ZnO and Bi_2O_3(5%)/ZnO exhibit good repeatability, though the responses are not high, see Figs. S6 and S7 (Supporting Information).

Moreover, Fig. 6a and b give the response time (τ_{res}) and recovery time (τ_{recov}) of the Bi_2O_3(3%)/ZnO and pristine ZnO sensors toward 100 ppm ethanol. As the results show, the τ_{res} of pristine ZnO sensor is 18 s, which is slower than that (7 s) of Bi_2O_3/ZnO sensor. The Bi_2O_3/ZnO sensor recover its initial state in a short time (τ_{recov} = 8 s). On the other hand, the ZnO sensor needs τ_{recov} = 23 s to recover. According to the recent literature, the τ_{res} and τ_{recov} of Bi_2O_3(3%)/ZnO sensor are smaller than that of pure ZnO, Bi_2O_3 and their respective composites, the details can be found in Table S1 (see Supporting Information). The results prove that the τ_{res} and τ_{recov} toward ethanol can be significantly improved by fabricating Bi_2O_3/ZnO nanocomposite, because the heterointerface between Bi_2O_3 phase and ZnO phase can well activate conductive electrons. Moreover, the long-term stability is another key index to gas sensor device [3,39]. To evaluate the life span of Bi_2O_3/ZnO, the Bi_2O_3/ZnO sensor was exposed to 100 ppm ethanol for 7 cycles in 60 days. Obviously, the response of the Bi_2O_3(3%)/ZnO sensor basically remains original level, see Fig. 6c, which manifests that the Bi_2O_3/ZnO sensor has excellent long-term stability towards ethanol. On the other hand, excellent selectivity is another important characterization for sensor because it enables the sensor to exclusively response to one gas and run for a long time to reduce the cost of device [49,50]. Significantly, the Bi_2O_3/ZnO sensor displays an excellent selectivity to ethanol compare to the same concertration of 100 ppm tested gases (*n*-hexane, chloroform, isopropanol, ethanol, benzene, methanol) at 175 °C, as illustrated in Fig. 6d. Clearly, the maximum gas response value of pristine ZnO toward alcohol is only 8.7, which is evidently lower than that (21.2) of

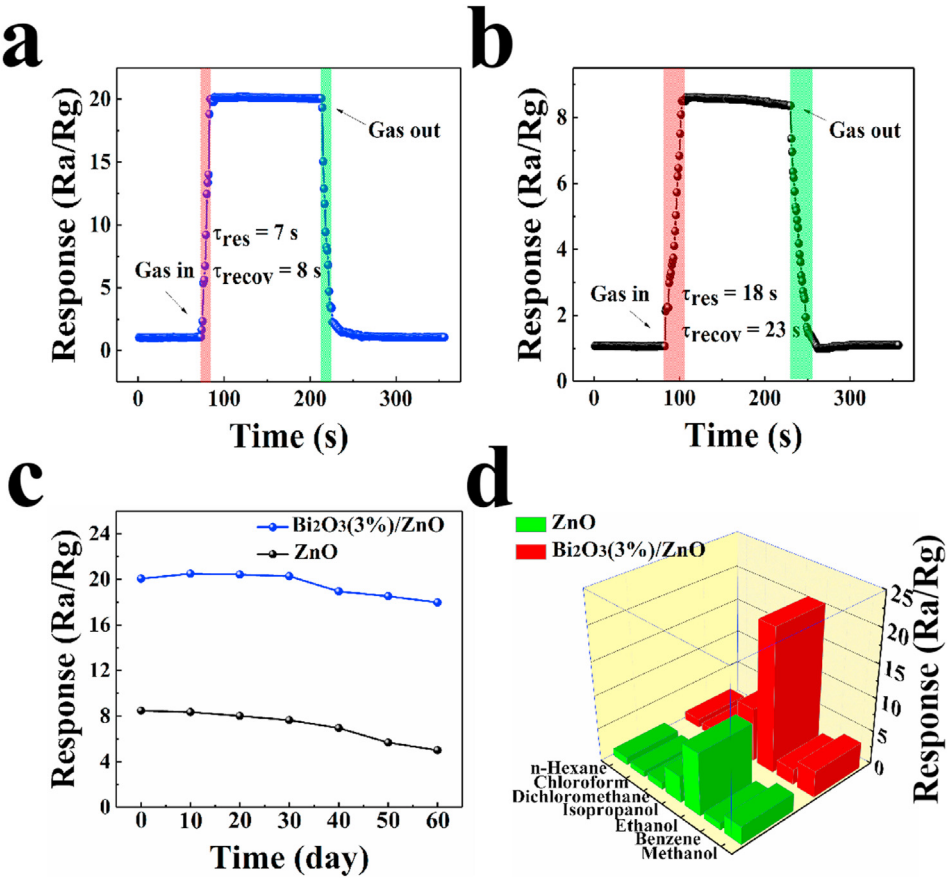

Fig. 6. (a) and (b) Dynamic resistance curves of the Bi_2O_3/ZnO and pure ZnO sensors toward 100 ppm ethanol at 175 °C and 250 °C, respectively; (c) Response stability of Bi_2O_3/ZnO and pure ZnO sensors toward ethanol at 175 °C and 250 °C lasting for 10, 20, 30, 40, 50, and 60 days, respectively. (d) The selectivity of the sensors based on Bi_2O_3/ZnO and pure ZnO to different gases with a concentration of 100 ppm at 175 and 250 °C, respectively.

Bi_2O_3/ZnO. According to our knowledge, the sensing selectivity may be influenced by the following three factors, such as reactive energy of VOC, operating temperature, and catalytic effect between Bi_2O_3 and ZnO heterophase [5,35]. Therefore, according to the above discussion, the superior performances exhibited by Bi_2O_3/ZnO sensor make it promising potential applications toward ethanol.

According to the previous literature, in order to explain the resistance-type gas sensing mechanism, the models of electron depletion layer (EDL) and electron accumulation layer (EAL) have been widely proposed by chemical adsorption and VOC gas molecule reaction at the surface of sensing material [2,5,39,51]. The Bi_2O_3 and ZnO are typical *p*-type and *n*-type MOSCs, respectively [36,52,53]. As Fig. 7a shows, the chemical adsorption/desorption of oxygen molecules or the VOC gas molecules on the materials' surface result in sharp alteration on the device resistance [5,54]. In fresh air, the O_2 molecules are chemiadsorbed on the surface of sensor, the O_2 capture the free electrons (e^{-1}) from conduction band, and the chemisorbed oxygen ion species such as O^-, O_2^-, and O^{2-} are genergeted, resulting in the formation of an EDL. On the other hand, the formation of the heterostructures, such as *p*-*n*, *p*-*p* and *n*-*n* can greatly increases the sensing performances and is closely related to the alterations in the EDL and EAL [49,55,56]. Though the enhanced sensing performance of the heterostructures has been extensively reported, the futher sensing mechanism on heterostructures is still need to be explored [57].

As shown in Fig. 7b and c, when two different MOSCs contact each other, e^{-1} flow from ZnO to Bi_2O_3 because the ZnO has a higher fermi energy (E_f) than that of Bi_2O_3 until the system reaches an equilibrium of E_f [10,48], and the energy band become bend. When the Bi_2O_3/ZnO nanocomposite is exposed in the air (Fig. 7a), the O_2 is adsorbed onto the surface of Bi_2O_3/ZnO nanocomposite, and capture e^{-1} from the MOSCs to generate oxygen species (O_2 (gas) → O_2 (ads), O_2 (ads) + e^- → O_2^- (ads), O_2^- (ads) + e^- → $2O^-$, O^- (ads) + e^- → O^{2-}(ads)) at the optimum working temperature of 175 °C [58]. Once the Bi_2O_3/ZnO nanocomposite is in the reducing gas of ethanol, the C_2H_6O molecules react with the adsorbed oxygen species, resulting in the widening of EDL at the interface between Bi_2O_3 and ZnO, the resistance of the Bi_2O_3/ZnO nanocomposite increases [59]. Thus, the response ($S_r = R_g/R_a$) of Bi_2O_3/ZnO in ethanol gas is significantly increased. In general, when two kinds of semiconductor metal oxides (SMOs) contact each other, the new equilibrium of E_f forms between Bi_2O_3 and ZnO interface due to the formation of heterojunctions [60]. The band bending and an additional EDL were caused by heterojunctions, leading to the device resistance increase in air and resistance greatly decrease in ethanol [59]. Finally, the response is significantly enhanced, and this reaction process with ethanol molecules is as the following equations of (1) and (2) [61]:

$$CH_3CH_2OH\ (ads) + 6O^-\ (ads) \rightarrow 2CO_2 + 3H_2O + 6e^- \quad (1)$$

$$CH_3CH_2OH\ (ads) + 6O^{2-}\ (ads) \rightarrow 2CO_2 + 3H_2O + 12e^- \quad (2)$$

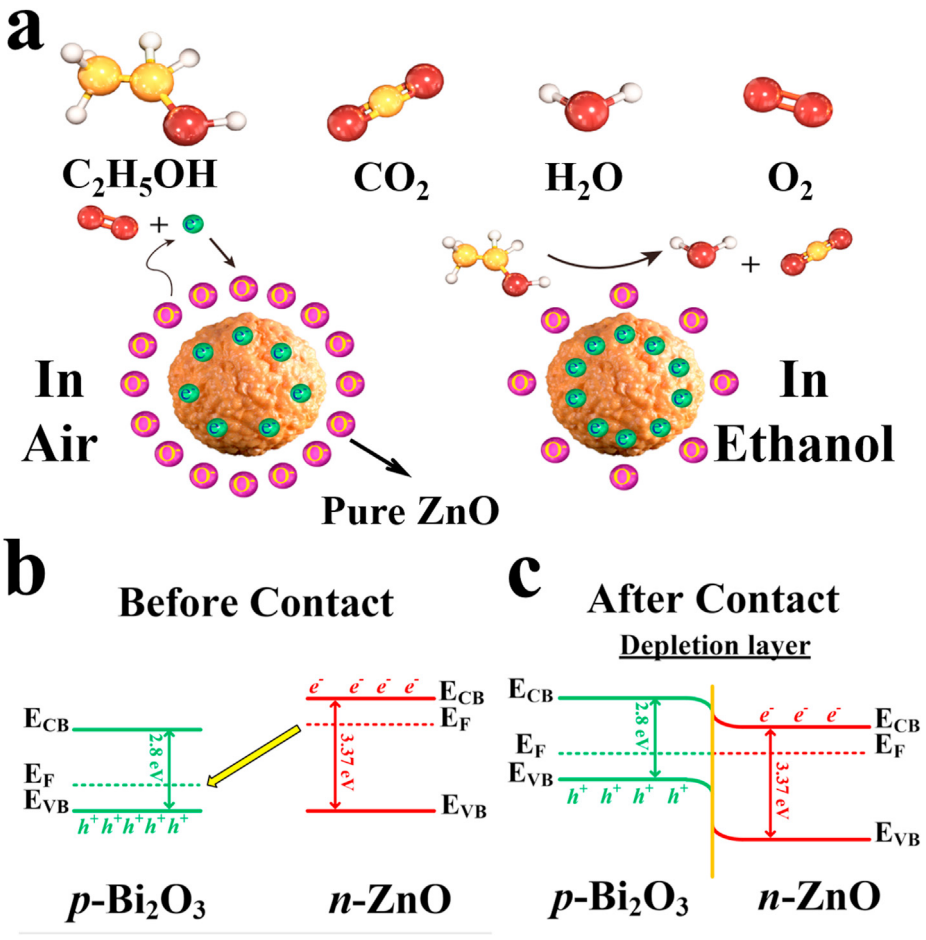

Fig. 7. (a) Schematic diagram of the sensing reaction mechanism of (a) gas sensing mechanism of Bi_2O_3/ZnO nanocomposite; Formation mechanism of the electron depletion layer formed at the *p*-*n* heterojunction energy band structure, (b) Before contact of *p*-type Bi_2O_3 and n-type ZnO, and (c) After contact of *p*-type Bi_2O_3 and *n*-type ZnO.

4. Conclusions

In summary, a novel heterostructured cauliflower Bi_2O_3/ZnO nanocomposite was synthesized by hydrothermal strategy. The Bi_2O_3/ZnO nanocomposite were utilized as a highly sensitive material, which exhibits excellent ethanol sensing performances, including enhanced gas response, low working temperature of 175 °C, wide concentration detection range from 1 to 500 ppm, excellent selectivity, and long-term stability with sensitive response and recovery, which is effective than that of pure ZnO based sensor or other nanocomposites of Bi_2O_3 and ZnO. The good sensing performances can be attributed to the heterostructure of *p*-Bi_2O_3/n-ZnO and the formation of tetragonal phase of β-Bi_2O_3. Therefore, the results would make a interesting contribution towards the fabrication of Bi_2O_3/ZnO based sensor. We believe that this low-cost, high-stability Bi_2O_3/ZnO nanocomposite will be one of the most promising sensing candidates for widely applications in ethanol detection.

CRediT authorship contribution statement

Peng Wang: Methodology, Validation, Investigation, Formal analysis, Writing - original draft. **Su-Zhen Wang:** Validation, Resources, Writing - review & editing. **Ya-Ru Kang:** Methodology, Validation. **Zhong-Sen Sun:** Methodology, Validation. **Xue-Dong Wang:** Investigation, Formal analysis. **Yu Meng:** Methodology, Validation. **Ming-Hui Hong:** Writing - review & editing. **Wan-Feng Xie:** Conceptualization, Investigation, Methodology, Writing - original draft, Writing - review & editing, Supervision.

Declaration of competing interest

The authors declare that they have no known competing financial interests or personal relationships that could have appeared to influence the work reported in this paper.

Acknowledgements

This work was financially supports from the National Natural Science Foundation of China (Grant No. 51227804), and the Natural Science Foundation of Jiangsu Province (BK20170330). This work was also funded by the Postdoctoral Scientific Research Foundation of Qingdao, and National College Students Innovation and Entrepreneurship Training Program of China (No.G201811065023). The authors would like to thank the Chemical Experimental Teaching Center of Qingdao University for the technique support, and Kehui Han from Shiyanjia Lab (m) for the TEM analysis.

Appendix A. Supplementary data

Supplementary data to this article can be found online at https://doi.org/10.1016/j.jallcom.2020.157152.

References

[1] B. Liu, Y.-M. Xu, K. Li, H. Wang, L. Gao, Y.-Y. Luo, G.T. Duan, Pd-catalyzed reaction-producing intermediate S on a Pd/In_2O_3 surface: a key to achieve the enhanced CS2-sensing performances, ACS Appl. Mater. Interfaces 11 (2019) 16838–16846.
[2] Y.H. Cho, X.-S. Liang, Y.-C. Kang, J.H. Lee, Ultrasensitive detection of trimethylamine using Rh-doped SnO_2 hollow spheres prepared by ultrasonic spray pyrolysis, Sens. Actuators, B 207 (2015) 330–337.
[3] L.-Z. Zhang, J.-N. Shi, Y.-H. Huang, H.-Y. Xu, K.-W. Xu, P.K. Chu, F. Ma, Octahedral SnO_2/Graphene composites with enhanced gas-sensing performance at room temperature, ACS Appl. Mater. Interfaces 11 (2019) 12958–12967.
[4] H.J. Chen, R.H. Bo, A. Shrestha, B.B. Xin, N. Nasiri, J. Zhou, I.D. Bernardo, A. Dodd, M. Saunders, J. Lipton-Duffin, T. White, T. Tsuzuki, A. Tricoli, NiO-ZnO nanoheterojunction networks for room-temperature volatile organic compounds sensing, Adv. Opt. Mater 6 (2018) 22.
[5] S. Park, S. Kim, G. Sun, C. Lee, Synthesis, structure, and ethanol gas sensing properties of In_2O_3 nanorods decorated with Bi_2O_3 nanoparticles, ACS Appl. Mater. Interfaces 7 (2015) 8138–8146.
[6] L. Zhu, W. Zeng, Y.-Q. Li, J.-D. Yang, Enhanced ethanol gas-sensing property based on hollow MoO_3 microcages, Physica E Low Dimens. Syst. Nanostruct 106 (2019) 170–175.
[7] S. Vallejos, I. Gracia, E. Figueras, C. Cané, Nanoscale heterostructures based on Fe_2O_3/WO_3-x nanoneedles and their direct integration into flexible transducing platforms for toluene sensing, ACS Appl. Mater. Interfaces 7 (2015) 18638–18649.
[8] C.-H. Feng, X. Li, J. Ma, Y.-F. Sun, C. Wang, P. Sun, J. Zheng, G.-Y. Lu, Facile synthesis and gas sensing properties of In_2O_3-WO_3 heterojunction nanofibers, Sens. Actuators, B 209 (2015) 622–629.
[9] L.F. da Silva, J.C. M'Peko, A.C. Catto, S. Bernardini, V.R. Mastelaro, K. Aguir, C. Ribeiro, E. Longo, UV-enhanced ozone gas sensing response of ZnO-SnO_2 heterojunctions at room temperature, Sens. Actuators, B 240 (2017) 573–579.
[10] F.-H. Zhang, Y.-C. Wang, L. Wang, J. Liu, H.-L. Ge, B. Wang, X.-Y. Huang, X.-D. Wang, Z.-T. Chi, W.-F. Xie, High performance $In_2(MoO_4)_3$/In_2O_3 nanocomposites gas sensor with long-term stability, J. Alloys Compd. 805 (2019) 180–188.
[11] Y.-C. Wang, Z.-S. Sun, S.-Z. Wang, S.-Y. Wang, S.-X. Cai, X.-Y. Huang, K. Li, Z.-T. Chi, S.-D. Pan, W.-F. Xie, Sub-ppm acetic acid gas sensor based on In_2O_3 nanofibers, J. Mater. Sci. 54 (2019) 14055–14063.
[12] C.-B. Zhai, M.-M. Zhu, L.-N. Jiang, T.-Y. Yang, Q. Zhao, Y. Luo, M.-Z. Zhang, Fast triethylamine gas sensing response properties of nanosheets assembled WO_3 hollow microspheres, Appl. Surf. Sci. 463 (2019) 1078–1084.
[13] S.-L. Peng, Z.-H. Wang, R. Liu, J. Bi, J.-T. Wu, Controlled oxygen vacancies of $ZnFe_2O_4$ with superior gas sensing properties prepared via a facile one-step self-catalyzed treatment, Sens. Actuators, B 288 (2019) 649–655.
[14] L. Liu, Y.-T. Zhao, P. Song, Z.-X. Yang, Q. Wang, Ppb level triethylamine detection of yolk-shell SnO_2/Au/Fe_2O_3 nanoboxes at low-temperature, Appl. Surf. Sci. 476 (2019) 391–401.
[15] Z.-J. Li, H. Li, Z.-L. Wu, M.-K. Wang, J.-T. Luo, H. Torun, P.-A. Hu, C. Yang, M. Grundmann, X.-T. Liu, Y.-Q. Fu, Advances in designs and mechanisms of semiconducting metal oxide nanostructures for high-precision gas sensors operated at room temperature, Mater. Horiz 6 (2019) 470–506.
[16] P. Cao, Z. Yang, S.T. Navale, S. Han, X. Liu, W. Liu, Y. Lu, F.-J. Stadler, D. Zhu, Ethanol sensing behavior of Pd-nanoparticles decorated ZnO-nanorod based chemiresistive gas sensors, Sens. Actuators, B 298 (2019) 126850.
[17] H.-R. Yang, X.-J. Bai, P. Hao, J. Tian, Y.-Y. Bo, X.-Z. Wang, H. Liu, A simple gas sensor based on zinc ferrite hollow spheres: highly sensitivity, excellent selectivity and long-term stability, Sens. Actuators, B 280 (2019) 34–40.
[18] H. Li, S.-S. Chu, Q. Ma, Y. Fang, J.-P. Wang, Q.-D. Che, G. Wang, P. Yang, Novel construction of morphology-tunable C-N/SnO_2/ZnO/Au microspheres with ultrasensitivity and high selectivity for triethylamine under various temperature detections, ACS Appl. Mater. Interfaces 11 (2019) 8601–8611.
[19] E.-X. Wu, Y. Xie, B. Yuan, H. Zhang, X.-D. Hu, J. Liu, D.-H. Zhang, Ultrasensitive and fully reversible NO_2 gas sensing based on *p*-type $MoTe_2$ under ultraviolet llumination, ACS Sens. 3 (2018) 1719–1726.
[20] A.A. Mane, A.V. Moholkar, Palladium (Pd) sensitized molybdenum trioxide (MoO_3) nanobelts for nitrogen dioxide (NO_2) gas detection, Solid State Electron. 139 (2018) 21–30.
[21] Y.K. Moon, S.Y. Jeong, Y.C. Kang, J.H. Lee, Metal oxide gas sensors with Au nanocluster catalytic overlayer: toward tuning gas selectivity and response using a novel bilayer sensor design, ACS Appl. Mater. Interfaces 11 (2019) 32169–32177.
[22] K.H. Lee, B.Y. Kim, J.W. Yoon, J.H. Lee, Extremely selective detection of ppb levels of indoor xylene using $CoCr_2O_4$ hollow spheres activated by Pt doping, Chem. Commun. 55 (2019) 751–754.
[23] J.-P. Cheng, J. Wang, Q.-Q. Li, H.-G. Liu, Y. Li, A review of recent developments in tin dioxide composites for gas sensing application, J. Ind. Eng. Chem. 44 (2016) 1–22.
[24] K. Hua, M.-M. Cui, Z.-P. Luo, D. Fang, R. Bao, Q. Qi, J.-H. Yi, B.-S. Sun, C.-C. Chen, Fabrication of Zinc pyrovanadate ($Zn_3(OH)_2V_2O_7 \cdot 2H_2O$) nanosheet spheres as an ethanol gas sensor, J. Alloys Compd. 801 (2019) 581–588.
[25] J. Ding, J.-W. Zhu, P.-C. Yao, J. Li, H.-P. Bi, X. Wang, Synthesis of ZnO-Ag hybrids and their gas-sensing performance toward ethanol, Ind. Eng. Chem. Res. 54 (2015) 8947–8953.
[26] Z.-H. Wang, Z.-W. Tian, D.-M. Han, F.-B. Gu, Highly sensitive and selective ethanol sensor fabricated with In-doped 3DOM ZnO, ACS Appl. Mater. Interfaces 8 (2016) 5466–5474.
[27] D.-J. Wang, Y.-Z. Zhen, G.-L. Xue, F. Fu, X.-M. Liu, D.-S. Li, Synthesis of mesoporous Bi_2WO_6 architectures and their gas sensitivity to ethanol, J. Mater. Chem. C 1 (2013) 4153.
[28] X.-L. Deng, L.-L. Zhang, J. Guo, Q.-j. Chen, J.-M. Ma, ZnO enhanced NiO-based gas sensors towards ethanol, Mater. Res. Bull. 90 (2017) 170–174.
[29] Y.H. Choi, D.H. Kim, S.H. Hong, $CuBi_2O_4$ prepared by the polymerized complex method for gas sensing applications, ACS Appl. Mater. Interfaces 10 (2018) 14901–14913.
[30] S.S. Zahirullah, P. Immanuel, S. Pravinraj, P.F.H. Inbaraj, J.J. Prince, Synthesis and characterization of Bi doped ZnO thin films using SILAR method for ethanol sensor, Mater. Lett. 230 (2018) 1–4.
[31] M. Bonyani, J.K. Lee, G.J. Sun, S. Lee, T. Ko, C. Lee, Benzene sensing properties and sensing mechanism of Pd-decorated Bi_2O_3-core/ZnO-shell nanorods, Thin Solid Films 636 (2017) 257–266.
[32] S. Balachandran, M. Swaminathan, Facile fabrication of heterostructured

Bi_2O_3-ZnO photocatalyst and its enhanced photocatalytic activity, J. Phys. Chem. C 116 (2012) 26306–26312.
[33] S. Park, J. Jun, H.W. Kim, C. Lee, Preparation of one dimensional Bi_2O_3-core/ZnO-shell structures by thermal evaporation and atomic layer deposition, Solid State Commun. 149 (2009) 315–318.
[34] S. Park, H. Ko, S. Lee, H. Kim, C. Lee, Light-activated gas sensing of Bi_2O_3-core/ZnO-shell nanobelt gas sensors, Thin Solid Films 570 (2014) 298–302.
[35] C.-Z. Li, J.-Y. Zhang, J.-A. Yang, T.-M. Wang, X. Lv, Z.-L. Tang, Methods to improve the photocatalytic activity of immobilized ZnO/Bi_2O_3 composite, Appl. Catal. Gen. 402 (2011) 80–86.
[36] Z. Zhang, C. Shao, X. Li, C. Wang, M. Zhang, Y. Liu, Electrospun nanofibers of *p*-type NiO/*n*-type ZnO heterojunctions with enhanced photocatalytic activity, ACS Appl. Mater. Interfaces 2 (2010) 2915–2923.
[37] J. Xu, J.-Y. Liu, Facet-selective epitaxial growth of δ-Bi_2O_3 on ZnO nanowires, Chem. Mater. 28 (2016) 8141–8148.
[38] Y.-S. Xu, T.-T. Ma, L.-L. Zheng, Y.-Q. Zhao, X.-H. Liu, J. Zhang, Heterostructures of hematite-sensitized $W_{18}O_{49}$ hollow spheres for improved acetone detection with ultralow detection limit, Sens. Actuators, B 288 (2019) 432–441.
[39] J.-H. Bang, M.S. Choi, A. Mirzaei, Y.J. Kwon, S.S. Kim, T.W. Kim, H.W. Kim, Selective NO_2 sensor based on Bi_2O_3 branched SnO_2 nanowires, Sens. Actuators, B 274 (2018) 356–369.
[40] O. Lupan, V. Postica, M. Hoppe, N. Wolff, O. Polonskyi, T. Pauporté, B. Viana, O. Majérus, L. Kienle, F. Faupel, R. Adelung, PdO/PdO_2 functionalized ZnO: Pd films for lower operating temperature H_2 gas sensing, Nanoscale 10 (2018) 14107–14127.
[41] Z.-H. Xiao, L.-B. Kong, X.-L. Li, S.-J. Yu, X.-Y. Li, Y. Jiang, Z.-J. Yao, S. Ye, C.-H. Wang, T.-S. Zhang, K. Zhou, S.-A. Li, Recent development in nanocarbon materials for gas sensor applications, Sens. Actuators, B 274 (2018) 235–267.
[42] B. Li, J.-Y. Liu, Q. Liu, R.-R. Chen, H.-S. Zhang, J. Yu, D.-L. Song, J.-Q. Li, M.-L. Zhang, J. Wang, Core-shell structure of ZnO/Co_3O_4 composites derived from bimetallic-organic frameworks with superior sensing performance for ethanol gas, Appl. Surf. Sci. 475 (2019) 700–709.
[43] B. Lei, W. Cui, J.P. Sheng, H. Wang, P. Chen, J.Y. Li, Y.J. Sun, F. Dong, Synergistic effects of crystal structure and oxygen vacancy on Bi_2O_3 polymorphs: intermediates activation, photocatalytic reaction efficiency, and conversion pathway, Sci. Bull. 65 (2020) 467–476.
[44] H. Zhou, S.-T. Zhong, M. Shen, Y.-F. Yao, Composite soft template-assisted construction of a flower-like β-Bi_2O_3/$Bi_2O_2CO_3$ heterojunction photocatalyst for the enhanced simulated sunlight photocatalytic degradation of tetracycline, Ceram. Int. 45 (2019) 15036–15047.
[45] Y. Bian, Y.J. Ma, Y.Y. Shang, P.F. Tan, J. Pan, Self-integrated β-Bi_2O_3/$Bi_2O_{2.33}$@$Bi_2O_2CO_3$ ternary composites: formation mechanism and visible light photocatalytic activity, Appl. Surf. Sci. 430 (2018) 613–624.
[46] S.-L. Bai, K. Tian, H. Fu, Y.-J. Feng, R.-X. Luo, D.-Q. Li, A.-F. Chen, C.-C. Liu, Novel α-Fe_2O_3/$BiVO_4$ heterojunctions for enhancing NO_2 sensing properties, Sens. Actuators, B 268 (2018) 136–143.
[47] S.-K. Zhao, Y.-B. Shen, X.-X. Yan, P.-F. Zhou, Y.-Y. Yin, R. Lu, C. Han, B.-Y. Cui, D.-Z. Wei, Complex-surfactant-assisted hydrothermal synthesis of one-dimensional ZnO nanorods for high-performance ethanol gas sensor, Sens. Actuators, B 286 (2019) 501–511.
[48] X.-Y. Huang, Z.-T. Chi, J. Liu, D.-H. Li, X.-J. Sun, C. Yan, Y.-C. Wang, H. Li, X.-D. Wang, W.-F. Xie, Enhanced gas sensing performance based on *p*-NiS/*n*-In_2O_3 heterojunction nanocomposites, Sens. Actuators, B 304 (2020) 127305.
[49] X.-L. Yang, S.-F. Zhang, Q. Yu, L.-P. Zhao, P. Sun, T.-S. Wang, F.-M. Liu, X. Yan, Y. Gao, X.-S. Liang, S.-M. Zhang, G.-Y. Lu, One step synthesis of branched SnO_2/ZnO heterostructures and their enhanced gas-sensing properties, Sens. Actuators, B 281 (2019) 415–423.
[50] J. Wu, Z.-X. Wu, H.-J. Ding, X. Yang, Y.-M. Wei, M.-Q. Xiao, Z.-Q. Yang, B.-R. Yang, C. Liu, X. Lu, L. Qiu, X.-T. Wang, Three-dimensional-structured boron- and nitrogen-doped graphene hydrogel enabling high-sensitivity NO_2 detection at room temperature, ACS Sens. 4 (2019) 1889–1898.
[51] P. Li, H.-Q. Fan, Y. Cai, In_2O_3/SnO_2 heterojunction microstructures: facile room temperature solid-state synthesis and enhanced Cl_2 sensing performance, Sens. Actuators, B 185 (2013) 110–116.
[52] J.C. Medina, N.S. Portillo-Vélez, M. Bizarro, A. Hernández-Gordillo, S.E. Rodil, Synergistic effect of supported ZnO/Bi_2O_3 heterojunctions for photocatalysis under visible light, Dyes Pigments 153 (2018) 106–116.
[53] Y. Peng, M. Yan, Q.-G. Chen, C.-M. Fan, H.-Y. Zhou, A.-W. Xu, Novel one-dimensional Bi_2O_3-Bi_2WO_6 *p-n* hierarchical heterojunction with enhanced photocatalytic activity, J. Mater. Chem. 2 (2014) 8517–8524.
[54] M. Ikram, Y. Liu, H. Lv, L.-J. Liu, A.U. Rehman, K. Kan, W.-J. Zhang, L. He, Y. Wang, R.-H. Wang, K.-Y. Shi, 3D-multilayer MoS_2 nanosheets vertically grown on highly mesoporous cubic In_2O_3 for high-performance gas sensing at room temperature, Appl. Surf. Sci. 466 (2019) 1–11.
[55] G. Li, X. Zhang, H. Lu, C. Yan, K.-X. Chen, H.-B. Lu, J.-Z. Gao, Z.-B. Yang, G.-Q. Zhu, C.-L. Wang, Z. He, Ethanol sensing properties and reduced sensor resistance using porous Nb_2O_5-TiO_2 *n-n* junction nanofibers, Sens. Actuators, B 283 (2019) 602–612.
[56] S.-Y. Shi, F. Zhang, H.-M. Lin, Q. Wang, E.-B. Shi, F.-Y. Qu, Enhanced triethylamine-sensing properties of P-N heterojunction Co_3O_4/In_2O_3 hollow microtubes derived from metal–organic frameworks, Sens. Actuators, B 262 (2018) 739–749.
[57] M. Zervos, E. Leontidis, E. Tanasă, E. Vasile, A. Othonos, Sn:In_2O_3 and Sn:In_2O_3/NiS_2 core-shell nanowires on Ni, Mo foils and C fibers for H_2 and O_2 generation, J. Phys. Chem. C 121 (2017) 27839–27848.
[58] T.-J. Qi, X. Yang, J. Sun, Neck-connected ZnO films derived from core-shell zeolitic imidazolate framework-8 (ZIF-8)/ZnO for highly sensitive ethanol gas sensors, Sens. Actuators, B 283 (2019) 93–98.
[59] J.-N. Zhang, H. Lu, L.-Z. Zhang, D.-Y. Leng, Y.-Y. Zhang, W. Wang, Y. Gao, H.-B. Lu, J.-Z. Gao, G.-Q. Zhu, Z.-B. Yang, C.-L. Wang, Metal-organic framework-derived ZnO hollow nanocages functionalized with nanoscale Ag catalysts for enhanced ethanol sensing properties, Sens. Actuators, B 291 (2019) 458–469.
[60] X. Zhang, W.-Y. Lan, J.-L. Xu, Y.-T. Luo, J. Pan, C.-Y. Liao, L.-Y. Yang, W.-H. Tan, X.-T. Huang, ZIF-8 derived hierarchical hollow ZnO nanocages with quantum dots for sensitive ethanol gas detection, Sens, Actuators B 289 (2019) 144–152.
[61] Q. Chen, S.Y. Ma, X.L. Xu, H.Y. Jiao, G.H. Zhang, L.W. Liu, P.Y. Wang, D.J. Gengzang, H.H. Yao, Optimization ethanol detection performance manifested by gas sensor based on In_2O_3/ZnS rough microspheres Sens, Actuators B 264 (2018) 264–278.